J|A|C|S
ARTICLES

Quasi-2D XY Magnetic Properties and Slow Relaxation in a Body Centered Metal Organic Network of [Co_4] Clusters

Partha Mahata,[†] Srinivasan Natarajan,*[,†] Pierre Panissod,[‡] and Marc Drillon*[,‡]

Framework Solids Laboratory, Solid State and Structural Chemistry Unit, Indian Institute of Science,
Bangalore 560 012, India, and Institut de Physique et Chimie des Matériaux de Strasbourg,
UMR 7504 CNRS-Université de Strasbourg, BP 43, 67034 Strasbourg Cedex2, France

Received March 17, 2009; E-mail: snatarajan@sscu.iisc.ernet.in; marc-drillon@ipcms.u-strasbgr.fr

Abstract: Octahedral Co^{2+} centers have been connected by μ_3−OH and μ_2−OH_2 units forming [Co_4] clusters which are linked by pyrazine forming a two-dimensional network. The two-dimensional layers are bridged by oxybisbenzoate (OBA) ligands giving rise to a three-dimensional structure. The [Co_4] clusters bond with the pyrazine and the OBA results in a body-centered arrangement of the clusters, which has been observed for the first time. Magnetic studies reveal a noncollinear frustrated spin structure of the bitriangular cluster, resulting in a net magnetic moment of 1.4 μB per cluster. For $T > 32$ K, the correlation length of the cluster moments shows a stretched-exponential temperature dependence typical of a Berezinskii−Kosterlitz−Thouless model, which points to a quasi-2D XY behavior. At lower temperature and down to 14 K, the compound behaves as a soft ferromagnet and a slow relaxation is observed, with an energy barrier of ca. 500 K. Then, on further cooling, a hysteretic behavior takes place with a coercive field that reaches 5 T at 4 K. The slow relaxation is assigned to the creation/annihilation of vortex−antivortex pairs, which are the elementary excitations of a 2D XY spin system.

Introduction

Since the early 1990s, the current trend toward ever-smaller electronic devices, which are based on spintronics, pushes the scientists to exploit the fascinating properties of the single-molecule magnets (SMM).[1] Exciting results have been reported for Mn_{12}[2] and Fe_8[3] molecular units, which offers the advantage of being perfectly defined in size, and to combine both the macroscopic properties of the classical magnets and the quantum ones of the nanoscale species.[4] These molecular systems exhibit below the blocking temperature a slow relaxation of the magnetization, and also a large hysteretic effect along with regular steps of the magnetization in terms of magnetic moment reversal by quantum tunneling. Such properties are directly related to a strong, Ising-like, anisotropy of the total spin of the cluster. More recently, slow relaxation of the magnetization was also observed in arrays of one-dimensional systems even below their 3D ordering temperature.[5]

As far as the 3D networks are concerned, the use of Euclidean geometry in a three-dimensional system of connected points provide, apart from their intrinsic interest and beauty, a clearer understanding of the complex connectivity in extended framework structures. This description provides a simple and elegant way of representing structures by emphasizing relations between the building units that are not always apparent from the conventional description in terms of space groups and sets of equivalent points. The three-dimensional net based approach for the topological description of structures, originally proposed by Wells,[6] has been put to great use in recent times for the understanding of metal-organic framework (MOF) structures.[7] Thus, three-dimensional MOF structures based on diamond, α-Po, boracite, $CdSO_4$, NbO, perovskite, Pt_3O_4, PtS, pyrite, quartz, rutile, sodalite, $SrSi_2$ $ThSi_2$ have been realized.[8] In most of these structures, the connectivity is generally based on three, four, or six connected nodes. A eight connected node with a cubic geometry would be based on CsCl structure, of which there are not many examples known in MOFs.[9] Schröder and co-workers reported the first crystal engineered CsCl type networks based on lanthanides using 4,4′-bipyridine-*N*,*N*′-dioxide as bridging ligand.[9a] Subsequently, the CsCl topology

---

[†] Indian Institute of Science.

[‡] Université de Strasbourg.

(1) Bogani, L.; Wernsdorfer, W. *Nat. Mater.* **2008**, *7*, 179.

(2) Sessoli, R.; Tsai, H.-L.; Schake, A. R.; Wang, S.; Vincent, J. B.; Folting, K.; Gatteschi, D.; Christou, G.; Hendrickson, D. N. *J. Am. Chem. Soc.* **1993**, *115*, 1804.

(3) (a) Wieghardt, K.; Pohl, K.; Jibril, I.; Huttner, G. *Angew. Chem., Int. Ed.* **1984**, *23*, 77. (b) Delfs, C.; Gatteschi, D.; Pardi, L.; Sessoli, R.; Wieghardt, K.; Hanke, D. *Inorg. Chem.* **1993**, *32*, 3099.

(4) Gatteschi, D.; Sessoli, R. *Angew. Chem., Int. Ed.* **2003**, *42*, 268.

(5) (a) Caneschi, A.; Gatteschi, D.; Lalioti, N.; Sangregorio, C.; Sessoli, R.; Venturi, G.; Vindigni, A.; Rettori, A.; Pini, M. G.; Novak, M. A. *Angew. Chem., Int. Ed.* **2001**, *40*, 1760. (c) Ishii, N.; Okamura, Y.; Chiba, S.; Nogami, T.; Ishida, T. *J. Am. Chem. Soc.* **2008**, *130*, 24. (d) Sessoli, R. *Angew. Chem., Int. Ed.* **2008**, *47*, 5508.

(6) Wells, A. F. *Three-Dimensional Nets and Polyhedra*; Wiley: New York, 1977.

(7) (a) Yaghi, O. M.; Li, H.; Davis, C.; Richardson, D.; Groy, T. L. *Acc. Chem. Res.* **1998**, *31*, 474. (b) Batten, S. R.; Robson, R. *Angew. Chem., Int. Ed.* **1998**, *37*, 1460. (c) Hill, R. J.; Long, D. L.; Champness, N. R.; Hubberstey, P.; Schröder, M. *Acc. Chem. Res.* **2005**, *38*, 337. (d) Chun, H.; Kim, D.; Dybtsev, D. N.; Kim, K. *Angew. Chem. Int. Ed* **2004**, *43*, 971.

(8) Öhrström, L.; Larsson, K. *Molecule-Based Materials, The Structural Network Approach*; Elsevier: Amsterdam, 2005.

(9) (a) Long, D. L.; Blake, A. J.; Champness, N. R.; Wilson, C.; Schröder, M. *Angew. Chem., Int. Ed.* **2001**, *40*, 2443. (b) Zhang, J.; Kang, Y.; Zhang, J.; Li, Z. J.; Qin, Y. Y.; Yao, Y. G. *Eur. J. Inorg. Chem.* **2006**, 2253.

10.1021/ja9017539 CCC: $40.75

has been observed for (Cu(isonicotinate)(nicotinate)) based on ($Cu_2(COO)_2O_2N_4$) unit as nodes.[9b]

Organic free radicals along with transition metal centers have been used for the rational design of new types of magnetic MOF structures.[10] The use of pyrazine as a ligand also give rise to magnetically interesting solids,[11] since it is known that pyrazine facilitates magnetic interactions and long-range ordering. The use of pyrazine to form magnetic solids was first established in $Cu(NO_3)_2$(pyrazine).[11a] Subsequently, Co(pyrazine)$_2$(NCS)$_2$,[11c] Fe(NCS)$_2$ (pyrazine)$_2$,[11d] [Cu(HF_2)(pyrazine)$_2$]BF_4,[11e] and [Cu(pyrazine)$_2$(ClO_4)$_2$],[11b,f] etc., were prepared, all of which show long-range magnetic ordering.

Since the discovery of the Mn_{12} SMM clusters, the organization of magnetic complexes using a variety of organic ligands resulted in a large number of transition metal cluster compounds with a wide variety of topologies, nuclearities, and diverse magnetic properties.[12] The wheel-shaped topology of the SMM has fascinated scientists from across the disciplines for a number of reasons.[13] The Mn_{12} and Fe_8 clusters and other related analogues have been well studied and in this connection it may be of interest to note that there are only few cobalt based SMMs that have been prepared and characterized.[12a,14] The Co^{2+} generally exhibits large molecular anisotropy,[15] resulting in a limited number of high-nuclearity clusters.[14c]

The advent of MOFs in recent years has been a boon to synthetic chemists as it facilitates organizing unusual metal clusters. The earliest known and probably the most studied example of the metal clusters is the OZn_4 cluster observed in the MOF-5 structure.[16] In transition metal MOFs, a number of metal clusters have been encountered.[17−22] Of these, the M_3 clusters with M=Cr,[18a,b] Fe,[18c−e] Mn,[18f] Co,[18g,h] Ni,[18d] the M_4 clusters with M=Fe,[19] Co,[20] the Co_7 cluster,[21] and the Co_8 cluster[22] are important and appear to have unique structures. The intercluster interactions in many of these compounds are, however, negligible due to the large separations between clusters.

It occurred to us that a combination of metal clusters and a facilitator, such as pyrazine, would open up interesting possibilities for magnetism and related properties. Such attempts in metal−organic frameworks have not been reported yet in the literature. Presently, we have employed a long aromatic dicarboxylate ligand (4,4′-oxybis(benzoate)) (OBA) and pyrazine, which gave rise to an interesting solid, ($Co_2(\mu_3-OH)(\mu_2-H_2O)$(pyrazine)(OBA)(OBAH)), **I**. Here, Co_4 clusters, ($Co_4(\mu_3-OH)_2(\mu_2-H_2O)_2$), are connected by the pyrazine ligand forming two-dimensional arrays, which are pillared by the OBA units. The ($Co_4(\mu_3-OH)_2(\mu_2-H_2O)_2$) clusters act as a eight-connecting node (four with pyrazine and four with OBA) and form a body centered (BC) structure, which appears to be the first BC structure involving transition metal clusters.

Experimental Section

Materials. The reagents needed for the synthesis are $Co(OAc)_2\cdot 4H_2O$ (Ranbaxy (India), 98%), 4,4′-oxybis(benzoic acid), (Lancaster (U.K.), 99%), pyrazine (Lancaster (U.K), 99%), and NaOH (CDH (India), 98%). The water used was double distilled through a Millipore membrane.

Synthesis. A mixture containing $Co(OAc)_2\cdot 4H_2O$ (0.252 g, 1 mM), 4,4′-oxybis(benzoic acid) (0.26 g, 1 mM), pyrazine (0.081

---

(10) Maspoch, D.; Ruiz-Molina, D.; Wurst, K.; Domingo, N.; Cavallini, M.; Biscarini, F.; Tejada, J.; Rovira, C.; Veciana, J. *Nat. Mater.* **2003**, *2*, 190.

(11) (a) Santoro, A.; Mighell, A. D.; Reimann, C. W. *Acta Crystallogr., Sect.: Struct. Sci.* **1970**, *26*, 979. (b) Darriet, J.; Haddad, M. S.; Duesler, E. N.; Hendrickson, D. N. *Inorg. Chem.* **1979**, *18*, 2679. (c) Lloret, F.; Munno, G. D.; Julve, M.; Cano, J.; Ruiz, R.; Caneschi, A. *Angew. Chem., Int. Ed.* **1998**, *37*, 135. (d) Bordallo, H. N.; Chapon, L.; Manson, J. L.; Hernandez-Velasco, J.; Ravot, D.; Reiff, W. M.; Argyriou, D. N. *Phys. Rev. B.* **2004**, *69*, 224405. (e) Manson, J. L.; Conner, M. M.; Schlueter, J. A.; Lancaster, T.; Blundell, S. J.; Brooks, M. L.; Pratt, F. L.; Papageorgiou, T.; Bianchi, A. D.; Wosnitza, J.; Whangbo, M. H. *Chem. Commun.* **2006**, 4894. (f) Lancaster, T.; Blundell, S. J.; Brooks, M. L.; Baker, P. J.; Pratt, F. L.; Manson, J. L.; Conner, M. M.; Xiao, F.; Landee, C. P.; Chaves, F. A.; Soriano, S.; Novak, M. A.; Papageorgiou, T. P.; Bianchi, A. D.; Herrmannsdörfer, T.; Wosnitza, J.; Schlueter, J. A. *Phys. Rev. B.* **2007**, *75*, 94421.

(12) (a) Yang, E.-C.; Hendrickson, D. N.; Wernsdorfer, W.; Nakano, M.; Zakharov, L. N.; Sommer, R. D.; Rheingold, A. L.; Gairaud, M.; Christou, G. *J. Appl. Phys.* **2002**, *91*, 7382. (b) Castro, S. L.; Sun, Z.; Grant, C. M.; Bollinger, J. C.; Hendrickson, D. N.; Christou, G. *J. Am. Chem. Soc.* **1998**, *120*, 2365. (c) Aubin, S. M. J.; Wemple, M. W.; Adams, D. M.; Tsai, H.-L.; Christou, G.; Hendrickson, D. N. *J. Am. Chem. Soc.* **1996**, *118*, 7746. (d) Milios, C. J.; Manoli, M.; Rajaraman, G.; Mishra, A.; Budd, L.; White, F.; Parsons, S.; Wernsdorfer, W.; Christou, G.; Brechin, E. *Inorg. Chem.* **2006**, *45*, 6782. (e) Yoo, J.; Wernsdorfer, W.; Yang, E. C.; Nakano, M.; Rheingold, A. L.; Hendrickson, D. N. *Inorg. Chem.* **2005**, *44*, 3377.

(13) (a) Cador, O.; Gatteschi, D.; Sessoli, R.; Larsen, F. K.; Overgaard, J.; Barra, A. L.; Teat, S. J.; Timco, G. A.; Winpenny, R. E. P. *Angew. Chem., Int. Ed.* **2004**, *43*, 5196. (b) Affronte, M.; Casson, I.; Evangilisti, M.; Candini, A.; Carreta, S.; Muryn, C. A.; Teat, S. J.; Timco, G. A.; Wernosdorfer, W.; Winpenny, R. E. P. *Angew. Chem., Int. Ed.* **2005**, *44*, 6496. (c) Waldmann, O.; Dobe, C.; Mutka, H.; Furrer, A.; Gudel, H. U. *Phys. Rev. Lett.* **2005**, *95*, 057202. (d) Waldmann, O. *Coord. Chem. Rev.* **2005**, *249*, 2550. (e) Tasiopolous, A.; Vinslava, A.; Wernsdorfer, W.; Abboud, K.; Christou, G. *Angew. Chem., Int. Ed.* **2004**, *43*, 2117. (f) Murugesu, M.; Wernsdorfer, W.; Abboud, K.; Christou, G. *Angew. Chem., Int. Ed.* **2005**, *44*, 892. (g) Shah, S. J.; Ramsey, C. M.; Heroux, K. J.; O'Brien, J. R.; DiPasquale, A. G.; Rheingold, A. L.; del Barco, E.; Hendrickson, D. N. *Inorg. Chem.* **2008**, *47*, 6245.

(14) (a) Zeng, M. H.; Yao, M. X.; Liang, H.; Zhang, W. X.; Chen, X. M. *Angew. Chem., Int. Ed.* **2007**, *46*, 1832. (b) Murrie, M.; Teat, S. J.; Stoeckli-Evans, H.; Güdel, H. U. *Angew. Chem., Int. Ed.* **2003**, *42*, 4653. (c) Boudalis, A. K.; Raptopoulou, C. P.; Abarca, B.; Ballesteros, R.; Chadlaoui, M.; Tuchagues, J. P.; Terzis, A. *Angew. Chem., Int. Ed.* **2006**, *45*, 432.

(15) (a) Oshio, H.; Nakano, M. *Chem.—Eur. J.* **2005**, *11*, 5178. (b) Oshio, H.; Hoshino, N.; Ito, T.; Nakano, M. *J. Am. Chem. Soc.* **2004**, *126*, 8805. (c) Ribas-Arino, J.; Baruah, T.; Pederson, M. R. *J. Am. Chem. Soc.* **2006**, *128*, 9497.

(16) Li, H.; Eddaoudi, M.; O'Keeffe, M.; Yaghi, O. M. *Nature* **1999**, *402*, 276.

(17) Ferey, G. *Chem. Soc. Rev.* **2008**, *37*, 191.

(18) (a) Ferey, G.; Serre, C.; Mellots-Draznieks, C.; Millange, F.; Surble, S.; Dutour, J.; Margiolaki, I. *Angew. Chem., Int. Ed.* **2004**, *43*, 6296. (b) Ferey, G; Mellot-Draznieks, C; Serre, C; Millange, F; Dutour, J; Surble, S; Margiolaki, I. *Science* **2005**, *309*, 2040. (c) Mellot-Draznieks, C.; Serre, C.; Surble, S.; Audebrand, N.; Ferey, G. *J. Am. Chem. Soc.* **2005**, *127*, 16273. (d) Jia, J.; Lin, X.; Wilson, C.; Blake, A. J.; Champness, N. R.; Hubberstey, P.; Walker, G.; Cussen, E. J.; Schröder, M. *Chem. Commun.* **2007**, 840. (e) Zheng, Y. Z.; Tong, M. L.; Xue, W.; Zhang, W. X.; Chen, X. M.; Grandjean, F.; Long, G. J. *Angew. Chem., Int. Ed.* **2007**, *46*, 6076. (f) Gutschke, S. O. H.; Molinier, M.; Powell, A. K.; Winpenny, R. E. P.; Wood, P. T. *Chem. Commun.* **1996**, 823. (g) Zhang, X. M.; Zheng, Y. Z.; Li, C. R.; Zhang, W. X.; Chen, X. M. *Cryst. Growth Des.* **2007**, *7*, 980. (h) Ma, L. F.; Wang, Y. Y.; Wang, L. Y.; Lu, D. H.; Batten, S. R.; Wang, J. G. *Cryst. Growth Des.* **2009**, *9*, 2036.

(19) Choi, S. B.; Seo, M. J.; Cho, M.; Kim, Y.; Jin, M. K.; Jung, D. Y.; Choi, J. S.; Ahn, W. S.; Rowsell, J. L. C.; Kim, J. *Cryst. Growth Des.* **2007**, *7*, 2290.

(20) (a) Luo, J.; Zhao, Y.; Xu, H.; Kinnibrugh, T. L.; Yang, D.; Timofeeva, T. V.; Daemen, L. L.; Zhang, J.; Bao, W.; Thompson, J. D.; Currier, R. P. *Inorg. Chem.* **2007**, *46*, 9021. (b) Xiang, S.; Wu, X.; Zhang, J.; Fu, R.; Hu, S.; Zhang, X. *J. Am. Chem. Soc.* **2005**, *127*, 16352. (c) Cheon, Y. E.; Suh, M. P. *Chem. Commun.* **2009**, 2296. (d) Liu, C. M.; Gao, S.; Zhang, D. Q.; Zhu, D. B. *Cryst. Growth Des.* **2007**, *7*, 1312.

(21) Cheng, X. N.; Zhang, W. X.; Lin, Y. Y.; Zheng, Y. Z.; Chen, X. M. *Adv. Mater.* **2007**, *19*, 1494.

(22) Zou, W. Q.; Wang, M. S.; Li, Y.; Wu, A. Q.; Zheng, F. K.; Chen, Q. Y.; Guo, G. C.; Huang, J. S. *Inorg. Chem.* **2007**, *46*, 6852.

g, 1 mM), and NaOH (0.08 g, 2 mM), and 10 mL of water was heated in a PTFE-lined stainless steel autoclave at 180 °C for 24 h to give brown crystals of I. (the yield was ~70% based on Co). The product was washed with deionized water under vacuum, and dried at ambient conditions. Elemental analysis Calcd (%) for **I**: C, 51.48; H, 3.22; N, 3.75. Found (%): C, 51.3; H, 3.15; N, 3.79.

Initial Characterization and Physical Measurements. Powder X-ray diffraction (XRD) patterns were recorded on well ground samples in the 2θ range 5−50° using Cu Kα radiation (Philips X'pert) (see Supporting Information (SI) Figure S1). The XRD patterns indicated that the product is a new material; the pattern being entirely consistent with the simulated XRD pattern based on the structure determined using the single-crystal XRD. The IR spectrum was recorded on a KBr pellet (Perkin-Elmer, SPECTRUM 1000) (see SI Figure S2). The thermogravimetric analysis (TGA) was carried out (Metler-Toledo) in oxygen atmosphere (flow rate = 20 mL/min) in the temperature range 30−850 °C (heating rate = 5 °C/min) (see SI, Figure S3). The TGA studies showed weight loss in two steps in the temperature range 200−440 °C. The total observed weight loss of 79% corresponds well with the loss of the pyrazine, the carboxylate, the OH and the water molecules (calc. 78.5%). The final calcined product was found to be crystalline by powder XRD and corresponds to Co_3O_4 (JCPDS: 42−1467).

Magnetic susceptibility measurements have been carried out on a Quantum Design MPMS-XL7 SQUID magnetometer between 4 and 300 K and in the range ± 50 kOe. AC susceptibility measurements have been performed at frequencies from 0.5 to 1500 Hz in an ac field of 3.5 Oe and in 0 applied dc field. All magnetic data have been corrected for the diamagnetic susceptibility 0.53×10^{-3} emu·cm^3·mol^{-1} computed from Pascal's tables and the demagnetizing effect, which reaches, at most, 10%.

Single-Crystal Structure Determination. A suitable single crystal was carefully selected under a polarizing microscope and glued carefully to a thin glass fiber. The single crystal data were collected on a Bruker AXS smart Apex CCD diffractometer at 293(2) K. The X-ray generator was operated at 50 kV and 35 mA using Mo Kα ($\lambda = 0.71073$ Å) radiation. Data were collected with ω scan width of 0.3°. A total of 606 frames were collected in three different setting of φ (0, 90, 180°) keeping the sample-to-detector distance fixed at 6.03 cm and the detector position (2θ) fixed at −25°. The data were reduced using SAINTPLUS,[23] and an empirical absorption correction was applied using the SADABS program.[24] The structure was solved and refined using SHELXL97[25] present in the WinGx suit of programs (Version 1.63.04a).[26] All the hydrogen atoms of the carboxylic acids were initially located in the different Fourier maps, and for the final refinement, the hydrogen atoms were placed in geometrically ideal positions and held in the riding mode. Final refinement included atomic positions for all the atoms, anisotropic thermal parameters for all the nonhydrogen atoms, and isotropic thermal parameters for all the hydrogen atoms. Full-matrix least-squares refinement against $|F|$ was carried out using the WinGx package of programs.[26] Details of the structure solution and final refinements is given in Table 1. CCDC: 676 900 contain the crystallographic data for this compound. These data can be obtained free of charge from The Cambridge Crystallographic Data Center (CCDC) via www.ccdc.cam.ac.uk/data_request/cif.

Results and Discussion

Structure. The asymmetric unit cell consists of two inequivalent Co^{2+} ions, Co(1) and Co(2) octahedrally coordinated, one dianionic OBA unit, one monoanionic OBAH unit, one pyrazine molecule, one μ_3−OH and one μ_2−H_2O molecule. Co(1) is coordinated by three carboxylate O atoms (Co(1)−O(1) = 2.011(2) Å, Co(1)−O(3) = 2.079(2) Å, Co(1)−O(4) = 2.153(2) Å), one μ_2−H_2O molecule (Co(1)−O(5) = 2.263(2) Å), and two μ_3−OH groups (Co(1)−O(2) = 2.0724(19) Å, Co(1)−O(2a) = 2.0691 (19) Å). Co(2) is coordinated by two carboxylate O atoms (Co(2)−O(6) = 2.061(2) Å, Co(2)−O(7a) = 2.066(2) Å), two nitrogen atoms from pyrazine (Co(2)-N(1a) = 2.146(3) Å, Co(2)−N(2) = 2.200(3) Å), one μ_2−H_2O molecule (Co(2)−O(5) = 2.212(2) Å) and one μ_3−OH group (Co(2)−O(2a) = 2.044(2) Å). (The selected bond distances are listed in SI Table S1). Among the two carboxylate units of the OBA, one has bidentate and the other has monodentate connectivity. OBAH, on the other hand, has only bidentate connectivity of one of the carboxylate and the other is a nonbonded acid group (see SI Figure S4).

Table 1. Crystal Data and Structure Refinement Parameters for ($Co_2(\mu_3$−OH)(μ_2−H_2O)(pyrazine)(OBA)(OBAH)), **I**[a]

structure parameter	I
empirical formula	$C_{32}H_{24}Co_2N_2O_{12}$
formula weight	745.866
crystal system	monoclinic
space group	$P2_1/c$ (no. 14)
a (Å)	11.173(3)
b (Å)	30.326(7)
c (Å)	9.645(2)
α (deg)	90.0
β (deg)	103.493(4)
γ (deg)	90.0
Volume (Å^3)	3178.0(13)
Z	4
T (K)	293(2)
ρ_{calc} (g cm^{-3})	1.559
μ (mm^{-1})	1.111
θ range (deg)	1.99 to 28.03
λ (Mo Kα) (Å)	0.71073
R indices (I > 2σ(I))	$R_1 = 0.0566$, w$R_2 = 0.1160$
R indices (all data)	$R_1 = 0.0846$, w$R_2 = 0.1279$

[a] $R_1 = \Sigma||_0|-|F_c||/\Sigma\ |F_0|$; w$R_2 = \Sigma(\mathrm{w}(F_0^2 - F_c^2)^2)/\Sigma(\mathrm{w}(F_0^2)^2))^{1/2}$. $w = 1/(\sigma^2(F_0)^2 + (aP)^2 + bP)$, $P = (\max.(F_0^2,0) + 2(F_c)^2)/3$, where $a = 0.0554$ and $b = 3.1192$.

The structure of the tetranuclear cobalt cluster [$Co_4(\mu_3$−OH$)_2$-(μ_2−$H_2O)_2$] is formed by two pairs of inequivalent cobalt (Co1,1a and Co2,2a) each pair being related by centrosymmetry in a bitrangular unit (Figure 1a). The μ_3−OH groups (O(2)) connect Co(1), Co(1a), and Co(2) or Co(2a). The μ_2−H_2O molecule (O(5)) connects Co(1) and Co(2) or Co(1a) and Co(2a) (Figure 1a). This connectivity results in three distinct nearest Co−Co distances: 3.059 Å (Co(1)−Co(1a)), 3.129 Å (Co(1)−Co(2) and Co(1a)−Co(2a)) and 3.624 Å (Co(1)−Co(2a) and Co(1a)−Co(2)) and four different Co−O−Co angles: 95.23° (Co(1)−O(2)−Co(1a) and Co(1)−O(2a)−Co(1a)), 88.74° (Co(1)−O(5)−Co(2) and Co(1a)−O(5a)−Co(2a)), 99.06° (Co(1)−O(2a)−Co(2) and Co(1a)−O(2)−Co(2a)), and 123.34° (Co(1a)−O(2a)−Co(2) and Co(1)−O(2)−Co(2a)).

In **I**, the [Co_4] clusters are connected by pyrazine molecule forming the two-dimensional layers (Figure 1b), which are pillared by OBA units giving rise to the three-dimensional structure (Figure 1c). As can be noted, the [Co_4] clusters are connected through four pyrazine and four OBA units to eight different [Co_4] clusters. The three-dimensional network can be simplified as uninodal eight-connected network based on the [Co_4] cluster as the node. Topological analysis shows that the Schläfli symbol for this network is $4^{24}.6^4$ and vertex symbol is

---

(23) *SMART (V 5.628), SAINT (V 6.45a), XPREP, SHELXTL*; Bruker AXS Inc.: Madison, WI, 2004.

(24) Sheldrick, G. M. *Siemens Area Correction Absorption Correction Program*; University of Göttingen: Göttingen, Germany, 1994.

(25) Sheldrick, G. M. *SHELXL-97 Program for Crystal Structure Solution and Refinement*; University of Göttingen, Göttingen: Germany, 1997.

(26) Farrugia, J. L. *J. Appl. Crystallogr.* **1999**, *32*, 837.

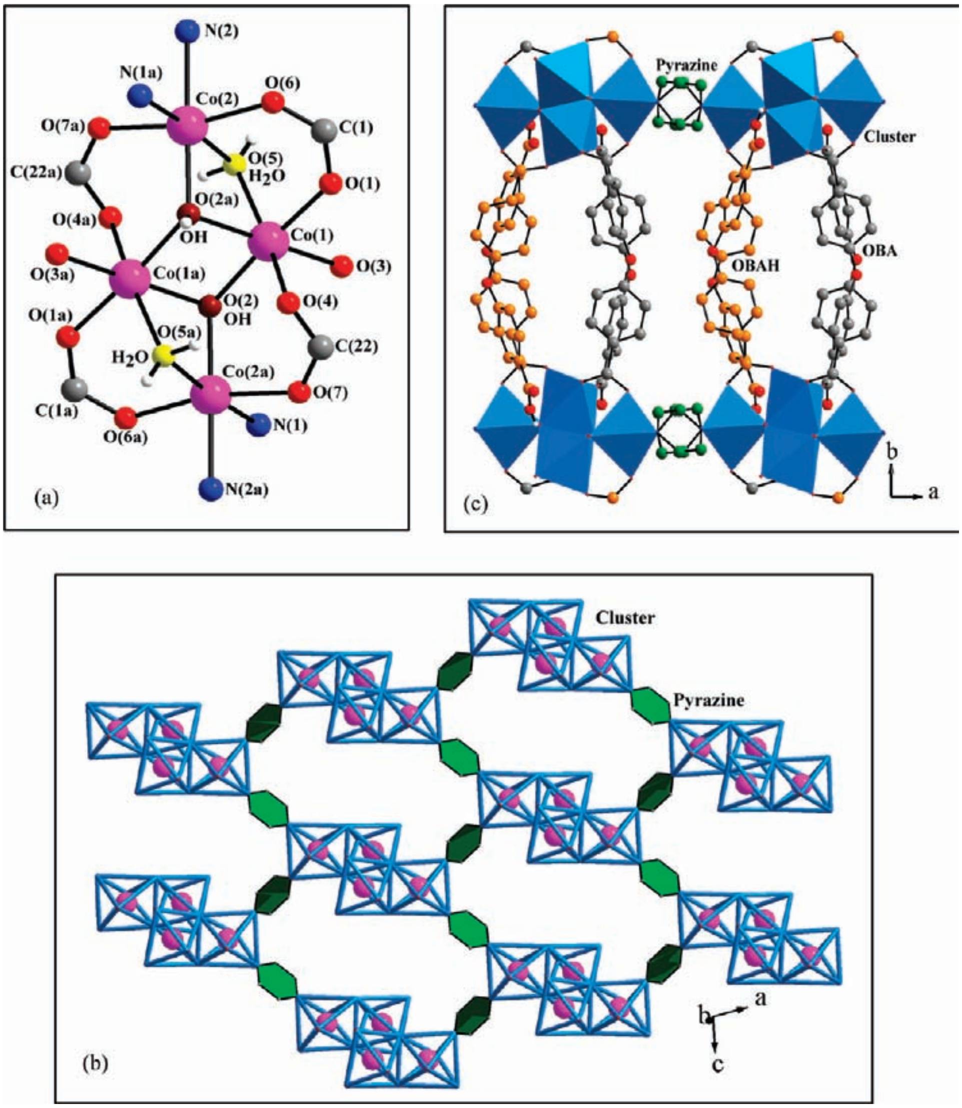

Figure 1. (a) Structure of the $(Co_4(\mu_3{-}OH)_2(\mu{-}H_2O)_2)$ cluster along with the coordination around Co^{2+} ions in $(Co_2(\mu_3{-}OH)(\mu_2{-}H_2O)(pyrazine)(OBA)(OBAH))$, **I**. (b) Two-dimensional connectivity between $[Co_4]$ clusters and pyrazine molecules. (c) Connectivity between two layers through OBA and OBAH unit to form the three-dimensional structure.

$4.4.4.4.4.4.4.4.4.4.4.4.4_3.4_3.4_3.4_3.4_3.4_3.4_3.4_3.4_3.4_3.4_3.4_3.*.*.*.*$. This arrangement is similar to that observed in the body-centered (BC) structures (Figure 2a). The present structure may be considered as being composed of two sets of (4,4) two-dimensional nets. Thus, one set of (4,4) net is parallel to the ac plane (pyrazine connected plane), whereas the other (4,4) net is parallel to the bc plane (OBA connected plane). The two mutually perpendicular nets are canted with respect to each other resulting in a eight-connected structure (Figure 2b).[9] This type of arrangement, not observed to date in transition metal containing MOFs, prompted us to investigate the magnetic behavior.

As mentioned before, metal clusters[16−22] have been assembled in metal−organic framework structure and it is not out of place to ponder over the formation of $[Co_4]$ clusters. In the present structure, the $[Co_4]$ clusters have been assembled in two dimensions employing the pyrazine organic ligand, and three-dimensionally through a carboxylate (OBA). We have earlier prepared and stabilized $[M_4]$ clusters,[28a] and in this sense the formation of $[Co_4]$ clusters is not completely unexpected. The formation of metal clusters connected either by oxygen or hydroxide ions, under hydrothermal conditions, would depend on the careful manipulations of many experimental parameters. It may be noted that many of the metal−organic frameworks are prepared employing soft-chemical approaches. It has also been shown that the hydro/solvothermal approach also provides a viable route for the preparation of MOF structures. The formation of a particular structure critically depends on the time and temperature of the reaction, the importance of which has been elegantly shown during the preparation of a series of cobalt succinate phases.[27c,d] In most of the cases, the lower temperatures generate molecular or low dimensional structures stabilized by extensive hydrogen bond interactions. On increasing the temperature, one observes the formation of higher dimensional structures with M−O(H)−M type linkages.[27,28] This is true for the reaction mixtures that are either neutral or slightly acidic. It has been observed that there is a tendency to form simple metal clusters at relatively low temperatures, which are generally not very stable at elevated temperatures. Since the hydrothermal method involves kinetically controlled reactions one needs to optimize the parameters to stabilize unusual clusters, which could be transient. It has been shown that the

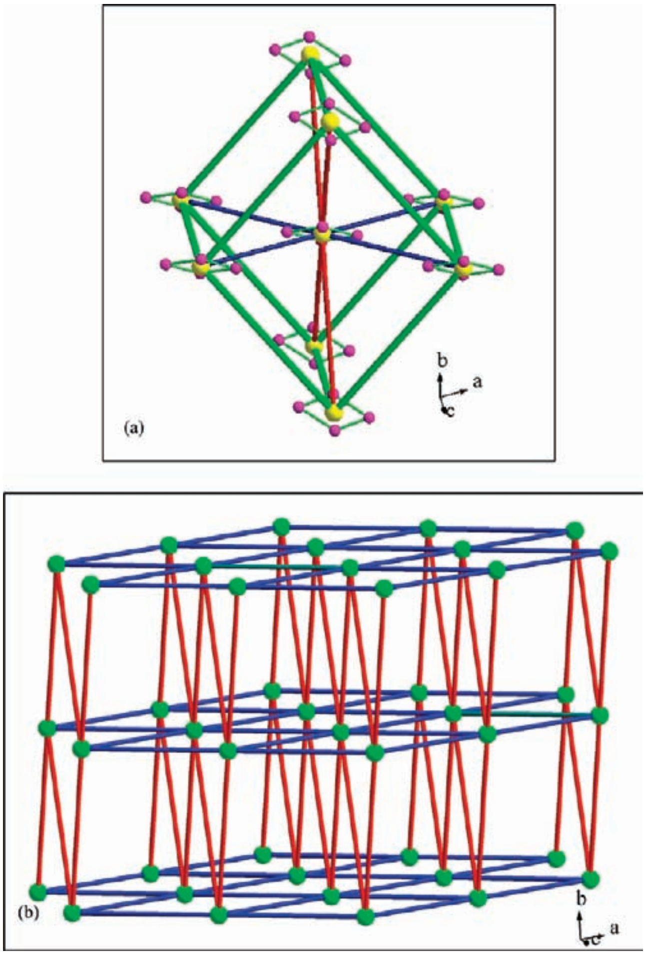

Figure 2. (a) Figure shows the body centered like unit based on the tetranuclear cluster connected through pyrazine (blue line) and OBA (red line) unit. (Yellow sphere-centroid of the $[Co_4]$ cluster, green line−cell edge of the elementary BC cell) (b) Three-dimensional connectivity of the cluster (green sphere) with pyrazine (blue line) and OBA unit (red line) to form two intersected (4,4) nets.

use of pyrazine and other related multitopic ligands help in stabilizing metal clusters of different shapes and sizes.[29] During the present study, the pyrazine, employed as the secondary base, binds with the $[Co_4]$ clusters and stabilizes them.

The macroscopic structure of the powdered samples is shown in the micrograph presented as Figure 3. Powder grains are needle shaped with a rather narrow distribution of diameter (~0.1 μm). However their length is broadly distributed from 0.1 to a few μm. The longitudinal axis of the needles is along the crystalline *b* axis. As will be shown later, this structure might have a significant impact on the magnetic properties because of finite size effects.

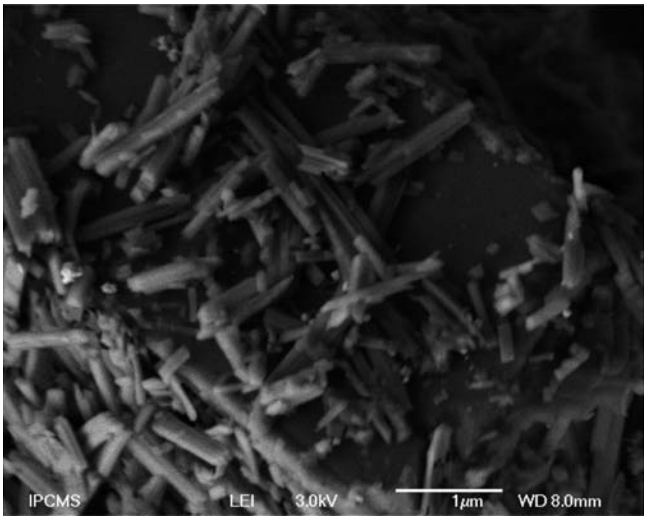

Figure 3. Micrograph of the powder sample showing the needle shape grains with a rather narrow diametrer distribution, about 0.1 μm, but a much larger length distribution, up to 2 μm.

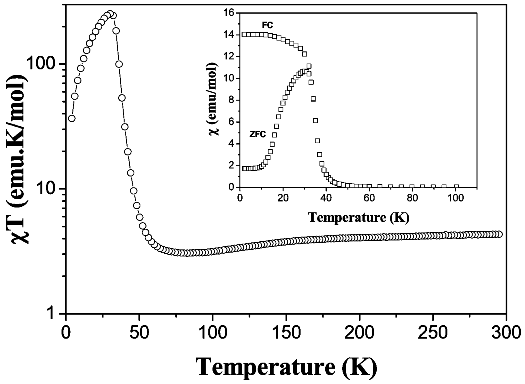

Figure 4. Temperature dependence of the χT product of **I**. Inset: the FC/ZFC curves in $H = 50$ Oe presented as a susceptibility (M/H) and showing, together with the steep increase of χT, the existence of a net moment of the cluster ground state and the occurrence of ferromagnetic order at 32 K.

Magnetic Properties. The dc magnetic susceptibility of **I** has been measured from 4 to 300 K in an applied field of 50 Oe (Figure 4). In the paper, unless otherwise specified, all magnetic data refer to the asymmetric unit cell, i.e., half a cluster or a Co(1)−Co(2) pair. At room temperature, the χT product (4.4 cm^{3}mol^{-1}K) is lower than the value usually observed for Co^{2+} ions (2.5−3 cm^3 mol^{-1} K per ion), which indicates a lower strength for the spin−orbit coupling. The observed value, however, is still larger than the spin only value of 1.9 cm^3 mol^{-1} K.

Upon cooling, the χT decreases to a minimum of 3 cm^3 mol^{-1} K at 80 K. Such a decrease is a characteristic effect of the spin−orbit coupling in Co^{2+} ions,[30] as well as the result of dominant antiferromagnetic (AF) exchange interactions (intra and/or inter clusters). Below 80 K, however, the χT product increases rapidly with decreasing T up to a maximum, which is about 2 orders of magnitude larger, around 30 K. This increase of χT is a clear signature that the cluster carries a net magnetic moment in its ground-state and that the clusters are ferromagnetically coupled to each other with a correlation length that increases steeply below 50 K. The plot of the field-cooled and the zero-field-cooled magnetic susceptibility confirms the stabilization of a magnetic state below ca. 32 K (inset Figure 4).

---

(27) (a) Mahata, P.; Prabu, M.; Natarajan, S. *Inorg. Chem.* **2008**, *47*, 8451. (b) Mahata, P.; Sundaresan, A.; Natarajan, S. *Chem. Commun.* **2007**, 4471. (c) Foster, P. M.; Stock, N.; Cheetham, A. K. *Angew. Chem., Int. Ed.* **2005**, *44*, 7608. (d) Foster, P. M.; Burbank, A. R.; Livage, C.; Ferey, G.; Cheetham, A. K. *Chem. Commun.* **2004**, 368.

(28) (a) Mahata, P.; Raghunathan, R.; Banerjee, D.; Sen, D.; Ramasesha, S.; Bhat, S. V.; Natarajan, S. *Chem. Asian. J.* **2009**, *4*, 936. (b) Mahata, P.; Sen, D.; Natarajan, S. *Chem. Commun.* **2008**, 1278.

(29) (a) Zhang, W.-H.; Song, Y.-L.; Ren, Z.-G.; Li, H.-X.; Li, L.-L.; Zhang, Y.; Lang, J.-P. *Inorg. Chem.* **2007**, *46*, 6647. (b) Nandini Devi, R.; Rabu, P.; Golub, V. O.; O'Connor, C. J.; Zubieta, J. *Solid State Sci.* **2002**, *4*, 1095.

(30) Curely, J.; Georges, R.; Drillon, M. *Phys. Rev. B.* **1986**, *33*, 6243.

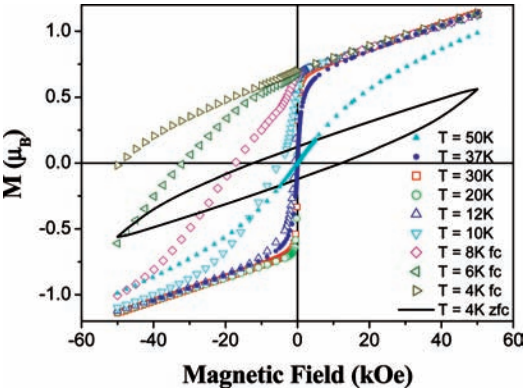

Figure 5. Magnetization curves M(H) observed for **I** showing a Langevin like behavior for $T > 32$ K (solid symbols), a soft ferromagnetic behavior for 14 K < T < 32 K (curves are superimposed in this temperature range) and a harder and harder ferromagnetic behavior for $T < 14$ K. Curves for $T < 10$ K have been recorded after cooling in a field of 50 kOe (see text). The curve recorded at 4 K after zero field cooling is shown as a solid line.

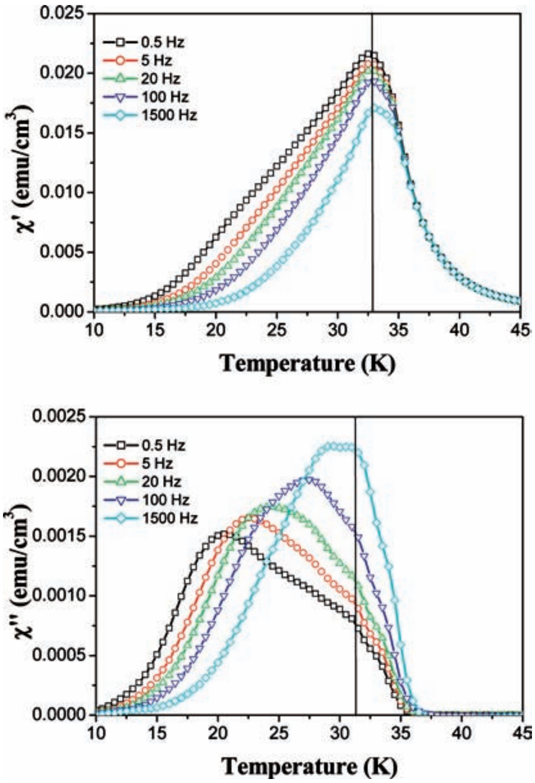

Figure 6. Temperature and frequency dependence of the ac susceptibility of **I** ($H_{ac} = 3.5$ Oe) (top) Real part, (bottom) Imaginary part. The frequency independent features (pointed by the vertical lines) show the occurrence of a phase transition at 32−33 K. The frequency dependent features (inflection point of χ' and maximum of χ" show the persistence of fluctuation/relaxation below the transition.

M(H) curves have been recorded from 50 to −50 kOe at temperatures below 50 K as shown in Figure 5. Below 10 K, the maximum available field was not sufficient to reach the reversible part of the loops (see, for instance, the loop measured at 4 K after cooling down the sample in zero field). In order to have a more correct view of the major loops, the measurements have been recorded after cooling the sample in the largest field (50 kOe) from 50 K down to the target temperatures, 10−4 K. Above 10 K the field cooled and the zero field cooled M(H) curves were found to be identical.

Between 50 and 30 K, the curves exhibit a Langevin like paramagnetic behavior, which confirms that a large number of clusters (hundreds to thousands, see next section) are ferromagnetically correlated. Between 30 and 20 K, all the M(H) curves appear to be the same. The M(H) behavior shows neither coercivity nor remanence and looks like that of a soft ferromagnet except for the linear, paramagnetic like, increase of M above 2 kOe. The extrapolated value of M at 0 field (1.4 μ_B per cluster) suggests either a ferrimagnetic arrangement between Co(1) and Co(2) with a slightly different g factor for the two nonequivalent Co sites or a noncollinear magnetic structure of the cluster.

Upon cooling below ca. 14 K, a hysteretic behavior is observed and the coercive field increases up to 50 kOe at 4 K, showing that two regimes, with and without hysteresis, may be identified in the temperature range 4−32 K. The rapid increase of the coercive field below 12 K can be related to the blocking of the residual thermal fluctuations present in the 15−32 K range. The very large coercive field observed at 4 K is likely to be related to the low net moment of the cluster together with a large magnetic anisotropy arising from the distortion of the pseudo-octahedral coordination of the magnetic Co(II) sites. Similar behavior has also been reported in a layered cobalt(II) terephthalate compound exhibiting a spin canted structure.[31]

The existence of a slow relaxation in the 15 K−32 K range is reflected in the frequency-dependence of the in-phase (χ') and the out-of-phase (χ'') magnetic susceptibility measured in an ac field of 3.5 Oe (Figure 6). Both χ' and χ'' show peaks in their temperature dependence that can be viewed as the signatures of the onset of long-range ordering, blocking or freezing of some dynamics, or even single molecule magnet (SMM)[32−34] characteristics. One can also observe that the peaks of $\chi'(T)$ and $\chi''(T)$ show completely different behaviors as a function of frequency. While the temperature at which $\chi'(T)$ peaks does not depend on frequency, the temperature for the χ"(T) maximum decreases steadily with decreasing frequency. In fact, a more closer look at the behavior shows that both $\chi'(T)$ and $\chi''(T)$ present two sets of singularities: (i) frequency independent singularities associated with a transition and (ii) frequency dependent singularities associated with some or several relaxation phenomena. The first set includes the maximum of $\chi'(T)$ at 32.5−33 K and a shoulder on the $\chi''(T)$ curves at 31−32 K, which eventually turns into a secondary maximum for the highest frequency.

From the very weak frequency shift of the χ' peak, at most 0.5 K, a maximum value of $\varphi = \Delta T_p/(T_p \cdot \Delta \log\omega) < 0.0044$ would be deduced, which lies in the usual range for spin-glasses.[32] However, it is difficult to imagine what kind of complex exchange frustration scheme could arise in a simple

---

(31) (a) Huang, Z. L.; Drillon, M.; Masciocchi, N.; Sironi, A.; Zhao, J. T.; Rabu, P.; Panissod, P. *Chem. Mater.* **2000**, *12*, 2805. (b) Rabu, P.; Drillon, M. *Adv. Eng. Mater.* **2003**, *5*, 189.

(32) Mydosh, J. A. *Spin Glasses: An Experimental Introduction*; Taylor & Francis: London, 1993.

(33) Coulon, C.; Miyasaka, H.; Clérac, R. *Struct. Bonding (Berlin)* **2006**, *122*, 163.

(34) (a) Powell, G. W.; Lancashire, H. N.; Brechin, E. K.; Collison, D.; Heath, S. L.; Mallah, T.; Wernsdorfer, W. *Angew. Chem., Int. Ed.* **2004**, *43*, 5772. (b) Novak, M. A.; Folly, W. S. D.; Sinnecker, J. P.; Soriano, S. *J. Magn. Magn. Mater.* **2005**, *294*, 133.

(35) (a) Drillon, M.; Panissod, P. *J. Magn. Magn. Mater.* **1998**, *188*, 93. (b) Laget, V.; Rouba, S.; Rabu, P.; Hornick, C.; Drillon, M. *J. Magn. Magn. Mater.* **1996**, *154*, L7.

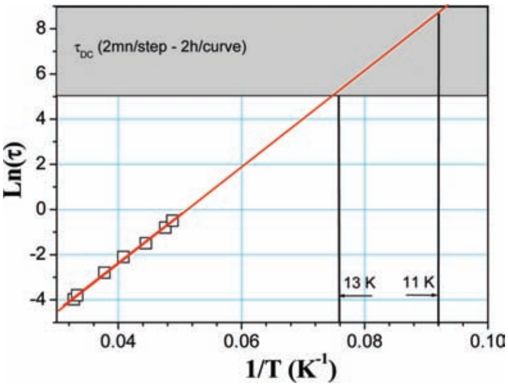

Figure 7. Arrhenius plot of the relaxation time deduced from the frequency dependent peak of χ''_{ac}. The grayed area is the time domain of the dc measurements showing that relaxation effects must be quenched at this time scale below ca. 12 K, in agreement with the observations.

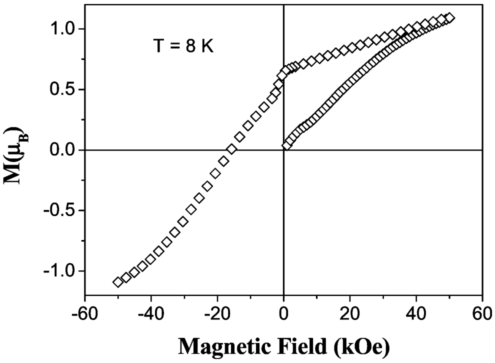

Figure 8. The figure shows the inhomogeneous (two steps) first magnetization and magnetization reversal of the system at 8 K showing the coexistence of soft and hard ferromagnetic character attributed to the length distribution of the needle shaped powder grains.

quasi-square network of equivalent clusters tetra-bonded by the same pyrazine ligands. The weak frequency shift that is observed is much more likely due to the overlap with the frequency dependent low temperature tail of χ'. Consequently, this first set of singularities is assigned to the critical slowing down around a transition. The second frequency dependent set, is characterized by the dominant maximum of $\chi''(T)$ and the corresponding inflection point that shifts on the low T side of $\chi'(T)$. By contrast, the shift in frequency of the second peak of $\chi''(T)$ is large and the value of the Mydosh parameter, about 0.1, is compatible with the blocking of a magnetization reversal mechanism. The frequency dependence of this latter peak in the temperature range 20.5−30.5 K has been analyzed in terms of a thermally activated hopping between the two magnetic states according to $\tau = \tau_0 \exp(\Delta/T)$ where Δ is the energy barrier/gap between the two states. This analysis (Figure 7) yields a rather large $\Delta = 489$ K and $\tau_0 = 1.3 \times 10^{-11}$ s. At first sight, such values would be consistent with superparamagnetic or SMM blocking. A quick quantitative analysis, however, shows that the fluctuating volume is neither compatible with that of the powder particles nor with that of a single cluster. Indeed from the spontaneous magnetization [Ms] of the sample, about 8 emu cm^{-3}, and a maximum coercive field ($H_C(T = 0)$ of 100 kOe) one can estimate the magnetic anisotropy constant, $K_A \sim M_S H_C$, ~800 KErg cm^{-3} (~8 K per cluster, namely ~2 K per ion). A model of thermally activated reversal above an anisotropy barrier $\Delta = K_A V_R \sim 490$ K would correspond to a reversal volume $V_R \sim 90$ nm^3 (60 clusters) to be compared with the volume of the particles (>10^5 nm^3) or the volume occupied by a single cluster (1.6 nm^3). This shows that the relaxation mechanism can be attributed neither to a superparamagnetic behavior of the powder particles nor to an SMM behavior.

The large overlapping between the frequency independent and frequency dependent peaks in the ac susceptibility studies, prevented us from performing a Cole−Cole analysis (χ'' vs χ') of the relaxation even at the lowest frequency. It must be noticed, though, that the blocking/freezing of the slow relaxation behavior occurs in an inhomogeneous way. Indeed, between 12 and 4 K, the M(H) curves (Figure 5) show that the magnetization reversal takes place in two steps: a fast reversal in low field (soft magnet behavior) followed by a much slower reversal in higher fields as T decreases (hard magnet behavior). As can be seen in Figure 8, the zero-field cooled first magnetization curve exhibits the same behavior with a first step in low field followed by a second slower increase in larger fields. In addition, the volume fraction of the soft (respectively hard) part decreases (respectively increases) with decreasing temperature (compare curves for 10, 8, and 6 K). Although the hypothesis of superparamagnetic blocking has been unambiguously rejected above, it seems clear that the distribution of the size (particularly of the length) of the needle shaped grains appears to play a significant role in the observed distribution of the blocking/freezing temperature.

From the above observations, different magnetic regimes have been considered upon cooling the sample: (i) In the high temperature paramagnetic regime, the magnetic behavior reflects the influence of dominant AF interactions within the cluster together with the effect of spin−orbit coupling at the Co(II) ions. These interactions result, at lower temperature, in a spin structure within the cluster that shows a net moment. The small value of the net moment (1.4 μ_B per [Co$_4$] cluster) points to either a ferrimagnetic configuration between Co(1)'s and Co(2)'s with a slightly different g factor or to a canted spin structure. (ii) Below 80 K, the rapid and large increase of χT shows that an extended spin correlation develops due to the presence of ferromagnetic exchange coupling between the clusters. On examination of the structure, it can be figured out that the pyrazine ligands could have the dominant influence on the observed magnetic behavior and favor a two-dimensional character. The exchange, through OBA, or dipolar interactions between the planes[35] are quite certainly much weaker. (iii) Upon cooling further, a ferromagnetic-like transition is observed at ca. 32.0 K, but below this transition, the ac susceptibility data and the absence of remnant magnetization point to the existence of residual spin fluctuations. This slow relaxation regime is assigned to the thermal hopping between two collective magnetic states with an energy barrier or gap of $\Delta \sim 500$ K. Indeed, the volume involved in this hopping is much larger than that of a single cluster (SMM behavior), but much smaller than the powder grains (superparamagnetic behavior). Therefore the origin of the fluctuations has to be found at some intermediate scale/dimension between the microscopic/0D SMM and the macroscopic/3D particles. (iv) Below ca. 12 K, the relaxation slows down to characteristic times that are longer than the experimental time and a hysteretic behavior takes place.

Analysis and Discussion of the Magnetic Properties. In order to rationalize the experimental results reported above it can be devised, as a work assumption, that the strength of the various exchange interactions can be sorted in decreasing order as intracluster (O mediated), intercluster (pyrazine mediated) in the ac plane, and interlayer (OBA mediated and/or dipolar).

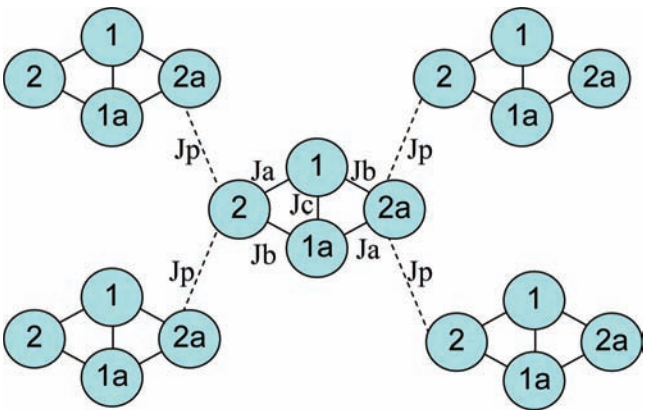

Figure 9. Scheme of the intracluster and intercluster exchange interactions in the ac plane. The different intracluster exchange bonds, Ja, Jb, and Jc, comprise actually several exchange pathways through O(OH), $O(H_2O)$, and carboxyl. The intercluster exchange bond Jp is through the pyrazine cycle.

Accordingly, it is expected that, with decreasing temperature, spin correlation takes place first inside the cluster, which builds up the cluster spin structure and its net moment, then it extends to 2D (or 3D) leading presumably to magnetic ordering.

From the examination of the different exchange pathways inside the cluster, one can deduce three different exchange routes connecting the Co pairs: Ja for Co(1)−Co(2) and Co(1a)−Co(2a), Jb for Co(1)−Co(2a) and Co(1a)−Co(2), and Jc for Co(1)−Co(1a). The Co(2) and Co(2a) are not directly coupled to each other but they are connected to the neighboring clusters through the pyrazine with a corresponding coupling strength Jp. This coupling scheme is shown in Figure 9. As mentioned in the previous section, the presence of a net moment in the ground state of the cluster shows that its spin structure is either ferrimagnetic or canted. The linear increase of M(H) above 2 kOe, however, can result only from the progressive closure of a spin fan in a noncollinear spin structure. The possibility of a paramagnetic contribution from a small impurity phase can be excluded readily because the slope of this linear increase is temperature independent and its value would correspond to a susceptibility of 0.05 emu·mol^{-1}, which is unrealistic for Pauli paramagnetism. The presence of Dzyaloshinsikii−Moriya interaction[36] is also excluded because the cluster is centrosymmetric. Therefore, the noncollinear spin structure must arise from competing exchange interactions. From the viewpoint of exchange pathways (Figure 9), the cluster is formed out of two edge shared triangular units. As a result, the AF exchange interactions within the cluster are expected to favor frustrations in the triangles and the opening of a spin fan.

On the basis of classical spin analysis, it is possible to get a coarse view of the spin arrangement in the cluster and to estimate the strength of the three different exchange interactions at work. Given a set of interactions, Ja, Jb, and Jc, the magnetization curve M(H) observed in the 20−30 K range has been simulated by minimizing, for each value of H, the total energy (exchange and Zeeman) against the orientations of the four moments. Because the experimental curves do not show any effect of magnetic anisotropy, it is not necessary to introduce such energy terms in the calculation of total energy. However a very small uniaxial anisotropy of 0.001 K per ion was introduced in order to set an arbitrary absolute orientation of the overall spin structure. It is not necessary to involve the intercluster interaction, Jp, because it does not compete with the intracluster interactions. Indeed once the net moments of the clusters are aligned, i.e., above a few kOe, all moments in a cluster are aligned with the corresponding ones in the adjacent clusters. Hence, the contribution of Jp to the exchange energy is minimum and independent of the field. The classical moments were given a value of 3 μ_B. For each set of J's the field strength was varied from −50 to +50 kOe, which yielded the expected M(H) curve corresponding to the interaction set. This operation was repeated for different interaction sets until the calculated curve and the experimental one coincide. The results of the simulation are shown in Figure 10 and the compatible sets of interactions are listed in Table 2.

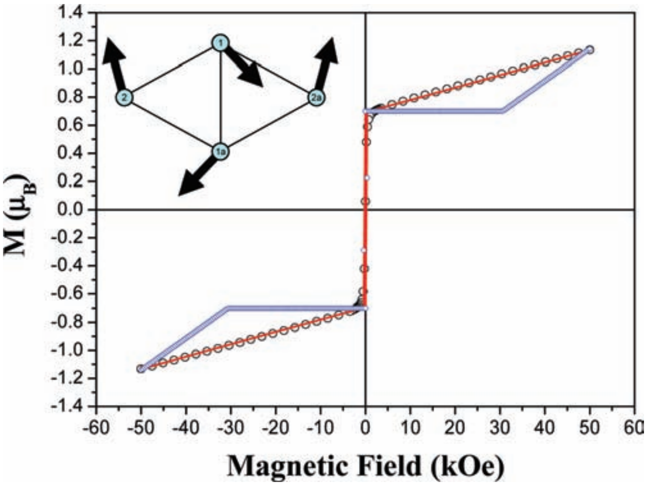

Figure 10. Result of the classical spin structure analysis. Symbols: the experimental curves at 20 K. Full line the best fit obtained from free energy minimization against the orientations of the four moments. The small symbol, blue curve shows that a collinear, ferrimagnetic structure cannot explain the observations. Inset: one of the possible canted spin structures compatible with the experimental curves. The corresponding exchange interaction strength Ja, Jb, Jc, and the angles are listed in Table 2.

Table 2. Results of a Classical Spin Analysis That Fit the Experimental M(H) Curves[a]

interaction set	Ja (K)	Jb (K)	Jc (K)	Co(2) angle	Co(2a) angle	Co(1) angle	Co(1a) angle
maximum	−25	−25	−31.5	0	0	−146.5	+146.5
typical	−33.5	−16.3	−29	+18.5	−18.5	−136	+136
minimum	−38	−12	−26	+38.4	−38.4	−123.8	+123.8

[a] The canted spin structure is necessary to reproduce the linear increase of M in large fields. It results from competing AF exchange interactions in the bi-triangular bond scheme (Figure 9). Ja and Jb may be swapped, of course. Minimum, typical, and maximum interaction sets stands for the value of the Jc/(Ja + Jb) ratio. The "minimum" value ∼1/2 of Jc/(Ja + Jb) is a threshold below which the canted structure with a net moment is no more stable. The "maximum" set corresponds to Ja = Jb for which the Co(2) moments are not canted. "Typical" corresponds to the scheme shown as an inset to Figure 10.

As can be seen, the classical analysis does not yield a unique set of interactions and angles, but a range with Ja + Jb about −50 K and Jc ranging from −26 to −32 K depending on the Ja/Jb ratio. Throughout the paper, J values are given in units of JS^2/k_B with J defined according to the Hamiltonian $H = -J\, S_i\, S_j$. For comparison, Figure 10 (blue curve) displays the simulation for a set of interactions (Ja, Jb < 0 and Jc > 0 arbitrary), which would result in a ferrimagnetic arrangement. Ja + Jb (−33 K) was adjusted to fit the experimental data at 50

---

(36) (a) Dzialoshinski, I. *J. Phys. Chem. Solids* **1958**, *4*, 241. (b) Moriya, T. *Phys. Rev. Lett.* **1960**, *4*, 5.

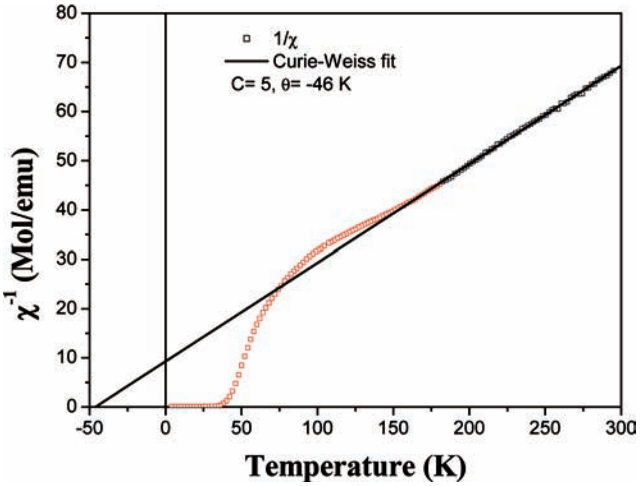

Figure 11. The Curie−Weiss plot of the dc susceptibility of **1**.

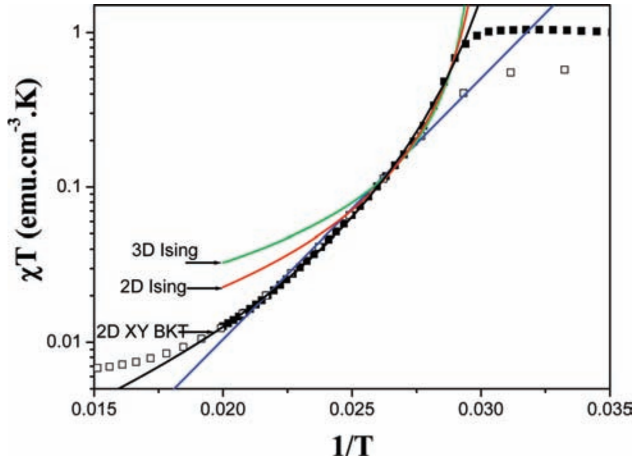

Figure 12. Semilog plot of the dc susceptibility as a function of the reciprocal temperature in the critical range 70−30 K. The susceptibility recorded in a field of 50 Oe (open squares) shows a mere noncritical exponential behavior. By contrast the susceptibility recorded in 2 Oe (solid squares), with a much slower cooling rate shows a critical upturn. Solid lines show the best fits, sorted by increasing quality, to the 3D Ising power law divergence ($\gamma = 1.25$, green) (3D XY or Heisenberg show comparable quality), 2D Ising power law divergence ($\gamma = 1.75$, red) and 2D XY (BKT, black) stretched exponential divergence. The critical temperatures are 32.3, 31.8, and 28.5 K, respectively. The straight blue line, ~exp(388/T), is the best noncritical fit (2D Heisenberg) to the data recorded in 50 Oe. Note that the semilog plot emphasizes the discrepancies for small values of χ.

kOe. Of course, in this latter case, Co(1) and Co(2) must be given a different moment (3 and 3.7 μ_B, respectively) to get the correct net moment in zero field. This analysis shows that, indeed, the canted spin structure of the cluster can only result from frustrated AF interactions in the triangles. The quantitative values that are deduced must be considered as indicative only, since they should be rescaled according to the actual values of the moments. It is shown below that the values are reasonably consistent with the average exchange interaction strength that can be estimated from the analysis of the high temperature data.

At high temperatures, χ^{-1} vs T shown in Figure 11 reveals a Curie−Weiss behavior with a Curie constant of 5 cm^3 mol^{-1} K and a Weiss temperature $\theta_W = -46$ K, which averages over the single ion spin−orbit interaction, the intracluster and intercluster interactions. For comparison, the classical spin analysis above yields an average value of <zJS^2≥−65 K for the intracluster interactions only. Theoretical approaches have been developed to deduce the effective exchange interaction in polynuclear clusters of hexacoordinated Co^{2+} which could possibly be compared to our estimate.[37] However, the interaction between cluster is far from being negligible in the present samples (see below), which might invalidate the approach. The Curie−Weiss law is no longer obeyed below 150 K due to the combined influence of the spin−orbit coupling and the increasing spin correlation within the cluster. The minimum observed for χT at 80 K suggests that the correlated spin state of the cluster may be provisionally considered as settled and the upturn of the susceptibility may be assigned to the intercluster interactions. The variation of χT in the range 50−30 K, for a dc field of 50 Oe, shows an approximately exponential increase (Figure 12). Such a noncritical behavior would contradict the raw observations of the ac susceptibility that shows the occurrence of a magnetic transition. It is known that finite field and time effects smear out the magnetic transitions. Therefore the dc measurements have been repeated with a much smaller field of 2 Oe, comparable to the ac field of 3.5 Oe, with a step of 0.5 K and a cooling rate 10 times smaller than the first measurement. The second curve shows indeed a clear upturn with respect to the exponential growth, which confirms the existence of a critical slowing down near the transition. The 2D or 3D nature of the transition was examined in the critical regime assuming, first, an Ising character for the effective spin of the cluster. Figure 12 shows two fits in the narrow critical range for a 2D Ising transition (fixed $\gamma = 1.75$) and a 3D Ising transition (fixed $\gamma = 1.25$). The best Tc values are 31.8 and 32.3 K, respectively. One can see that the 2D transition gives a slightly better fit but the comparison is not conclusive.

By contrast, an excellent fit could be obtained over the whole 50−32 K range using the Berezinskii−Kosterlitz−Thouless (BKT)[38] critical expression for χT, namely

$$\chi T = a e^{b/\sqrt{T-T_{\mathrm{BKT}}}} \text{ with } T_{\mathrm{BKT}} = 28.5\ \mathrm{K},$$
$$a = 0.14 \times 10^{-3}\,\mathrm{emu\ cm^{-3}\ K} \text{ and } b = 20\ \mathrm{K}^{1/2}$$

which strongly suggests a 2D XY character of the cluster moment as a whole. Why would the global spin of the cluster behave as XY out of Ising like Co^{2+} ions? It can be seen from the structure (Figure 1a) that the coordination octahedra of Co(1) and Co(2) are quite differently oriented, which implies a different main anisotropy axis for the two nonequivalent Co^{2+} ions. In addition, the noncollinear spin structure of the cluster implies that there is no orientation of the net moment for which all spins can lie simultaneously along their easy axis. Consequently, even if Co^{2+} ions are Ising like the uniaxial anisotropy of the net moment is reduced with respect to that of four collinear spins. It is also possible, yet not frequently encountered, that Co^{2+} ions are XY like, depending on the distortion of their coordination octahedron. Therefore, it can be assumed with some confidence that the behavior of the net cluster spin is XY like. In addition, the existence of a BKT transition in the ac plane of **1** provides a straightforward explanation for the persistence of fluctuations even below the transition. Indeed below the transition, a BKT system remains critical down to $T = 0$ — there is no strict long-range order — and the average magnetization is 0 in the absence of magnetic field and of residual anisotropy

---

(37) (a) Lines, M. E. *J. Chem. Phys.* **1971**, *55*, 2977. (b) Lloret, F.; Julve, M.; Canon, J.; Ruiz-García, R.; Pardo, E. *Inorg. Chim. Acta* **2008**, *361*, 3432.

(38) (a) Berezinskii, V. L. *Zh. Eksp. Teor. Fiz.* **1970**, *59*, 1907. [Sov. Phys. JETP **1971**, *42*, 493]. (b) Kosterlitz, J. M.; Thouless, D. J. *J. Phys. C* **1973**, *6*, 1182. (c) Kosterlitz, J. M. *J. Phys. C* **1974**, *7*, 1046.

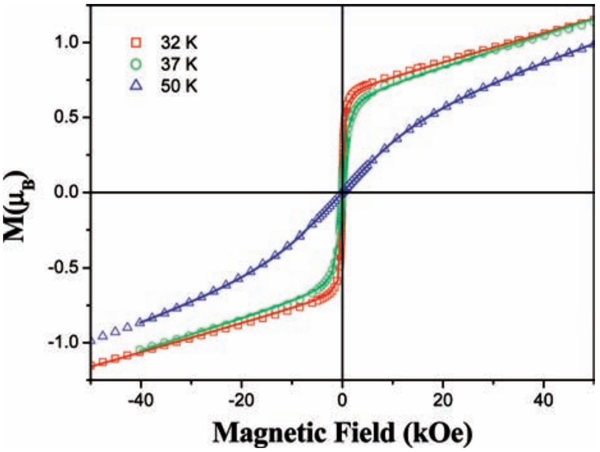

Figure 13. Langevin fits of the experimental M(H) curves above the transition temperature (see text).

in the XY plane. There is an apparent inconsistency, however, between the value of T_{BKT} (28.5 K) and the critical temperature indicated by the maximum of χ'_{ac} (~32.5 K). There are no theoretical studies of the ac susceptibility in BKT systems, but it is known that the specific heat peaks at a temperature that is 10−15% higher than T_{BKT} contrary to the cases of order−disorder transitions.[38−40] Whether this specificity of the BKT transition applies also to the dynamic susceptibility is an open question.

From the value of T_{BKT}, one can estimate the strength of the exchange interaction through the pyrazine bonds. Monte Carlo simulations for a classical XY spin[39] show that $T_{BKT} = 0.89$ JS^2 and for an anisotropic XXZ spin[40] $T_{BKT} = 0.70−0.55$ JS^2 depending on the Z/X spin anisotropy factor (from 0 to 0.99). Consequently the strength of Jp would lie between 32 and 52 K. For comparison in the classical 2D Ising model,[41] the transition temperature $T_C = 2.27$ $JS^2 = 33$ K would yield Jp = 14.5 K. Therefore, except if the transition is Ising like, which is not the preferred scenario, the cluster spin is probably not fully settled before the intercluster interactions start to play a significant part. That the situation is intricate can be shown independently by analyzing the M(H) curves above the transition. The M(H) curves can, indeed, be remarkably reproduced by Langevin curves with an additional paramagnet-like component to account for the closure of the cluster spin fan (Figure 13). The fits have been performed from 50 K down to 32 K, from which the net cluster moment and the number of correlated moments can be deduced independently as the prefactor and the argument of the Langevin function, respectively. The additional paramagnetic contribution is found to be the same as the one below the transition, which shows that the spin structure of the cluster is preserved through the transition. The number of correlated clusters Nc is found to increase approximately exponentially from 240 at 50 K to 5500 at 32 K. The net cluster moment, however, is also found to show a small variation from 1 μ_B at 50 K to the nearly maximum value of 1.38 μ_B at 32 K. This suggests that the intra- and the intercluster interactions work concurrently in the 80−32 K range. Close to the transition, Nc does not diverge but saturates to a value of 6000; this is expected because the analysis is essentially that of the high field data. Actually the exponential growth of Nc parallels that of the dc susceptibility measured in 50 Oe (Figure 12). The maximum value of Nc and the corresponding correlated surface area in the ac plane, about 6000 nm^2, call for an important remark: indeed, this correlated surface area is close to that of the cross-section of most needle-shaped grains, about 8000 nm^2. Therefore, finite size effects are likely to play a non-negligible part in the observed properties. In particular, the finite diameter of the grains is the most plausible explanation for the ac susceptibility peaking at a slightly higher temperature than the extrapolated BKT transition temperature.

The above analysis shows that **I** undergoes a magnetic transition at ca. 32 K, which can be either a 2D XY transition (preferred) or long-range Ising (in plane) one. It is clear that the magnetic measurements on a single crystal would decide between the two cases. Unfortunately, the preparation of a mm^3 single crystal seems out of reach with the synthesis process described above.

The last question to answer about the magnetic properties of the system is the origin of the slow fluctuations and their blocking/freezing below 14 K. In the previous section, we have discarded a superparamagnetic-like behavior of the single cluster or of the powder particles. If the net cluster moment has really an XY character, it is tempting to assign the relaxation to the reversal of individual ac disks in the particles. Unfortunately, the magnetic anisotropy barrier involved in the reversal of a single disk, the volume of which is about 12×10^3 nm^3 (i.e, 8000 clusters), is still much larger than the observed value, $\Delta = 490$ K. Hence, the origin of the relaxation must be found at some smaller scale, between that of a single cluster and a single disk. A classical explanation could be the nucleation of reverse domains with a volume of about $V_R \sim 90$ nm^3 around the structural defects or at the edge of the particles, followed by the domain wall propagation. This is the ordinary case for systems exhibiting a long-range order magnetic transition, 2D Ising or 3D like. Actually, the ac susceptibility curves observed in the present sample are quite similar, qualitatively, to those observed by Coronado et al. in the quasi-2D system $(Ni(chxn)_2)_3(Fe(CN)_6)_2 \cdot 2H_2O$, which is shown to undergo a 2D Ising transition.[42] Therefore the existence of such a transition in the present sample cannot be discarded. However, we propose an alternate explanation that involves the elementary excitations of a BKT system below the transition, namely the creation/annihilation of vortex/antivortex pairs. The energy cost 2 μ (μ = the chemical potential of a vortex) for the creation of such a pair is about 10 JS^2.[38] More recent Monte Carlo simulations suggest 2 $\mu \sim 7.5$ JS^2.[39] The values of JS^2 have been estimated above to lie between 32 and 52 K. Consequently the energy gap for the creation of an elementary BKT excitation would be in the range 240−520 K, which compares well with the large energy barrier $\Delta = 490$ K involved in the slow relaxation observed below the transition. One can, therefore, speculate that the slow relaxation finds its origin in the elementary excitations of a quasi-2D XY system, similarly to that recently proposed for the slow relaxation observed in quasi-1D Ising systems.[5] In the latter, the elementary excitations involved in the relaxation are those of the 1D Ising chain (Glauber[43] dynamics) and the energy gap is 2 JS^2, as compared to 7.5 to 10 JS^2 for the 2D system.

Summary and Conclusions

For the first time, a body centered network of $[Co_4]$ magnetic clusters has been synthesized. The inorganic cluster is formed

---

(39) Gupta, R.; Baillie, C. F. *Phys. Rev. B* **1992**, *45*, 2883.

(40) Cuccoli, A.; Tognetti, V.; Vaia, R. *Phys. Rev. B* **1995**, *52*, 10221.

(41) Onsager, L. *Phys. Rev.* **1944**, *65*, 117.

(42) Coronado, E; Gomez-Garca, C. J.; Nuez, A.; Romero, F. M.; Waerenborgh, J, C. *Chem. Mater.* **2006**, *18*, 2670.

(43) (a) Glauber, R. J. *J. Math. Phys.* **1963**, *4*, 294. (b) Zumer, S. *Phys. Rev. B* **1980**, *21*, 1298.

out of octahedral Co^{2+} centers connected by μ_3−OH and μ_2−OH_2 units resulting in a bitriangular [Co_4] arrangement. The clusters are linked by pyrazine to form a two-dimensional network in the ac plane of the crystal. In turn, the 2D layers are bridged by the oxy-bisbenzoate (OBA) ligands along the *b* crystal axis to build up the three-dimensional structure. The multidimensional structure of the network and the various exchange paths gives rise to a wealth of magnetic behaviors. As the temperature decreases, spin coherence builds up first inside the clusters through the oxygen bonds. The competing AF interactions within the triangles make the cluster to adopt a noncollinear spin structure with a net magnetic moment of 1.4 μ_B. This has been demonstrated by a classical analysis of the magnetization curves, the intracluster spin coherence being essentially settled below 50 K. The exchange coupling through pyrazine builds up a ferromagnetic correlation between the clusters, which results in a quasi 2D magnetic behavior in the ac layers. The system, eventually, undergoes a Berezinskii−Kosterlitz−Thouless transition at 32 K, which is evidenced by the stretched-exponential divergence of the magnetic susceptibility in low fields. BKT systems remain critical below the transition temperature and hence no hysteresis is observed in the magnetization curves down to 14 K. The possibility of a 2D Ising transition cannot be excluded, though. A thermally activated slow relaxation is observed with an energy barrier of ca. 500 K. The relaxation times, below 14 K, becomes long enough for the occurrence of coercivity in the M(H) curves with the coercive field reaching a value as high as 5 *T* at 4 K. Although the temperature dependence of the relaxation time could suggest either a superparamagnetic behavior of the powder particles or a single molecule magnet (SMM) behavior of the clusters, none of these effects can quantitatively explain the value of the activation energy. The estimated anisotropy barrier for a single cluster (8 K) is, indeed, much too small and, oppositely, the volume of the smallest particles is too large. By contrast, the value of the activation energy lies in the estimated energy range (240−520 K) of the vortex−antivortex elementary excitations of an XY system. It is then concluded, tentatively, that the observed slow relaxation is associated with the thermally activated creation/annihilation of the elementary excitations of an XY system.

Acknowledgment. S.N. thanks the Department of Science and Technology (DST), Government of India, for the award of a research grants, and we thank the Council of Scientific and Industrial Research (CSIR), Government of India, for the award of a fellowship (P.M.) and a research grant. S.N. also thanks the Department of Science and Technology, Government of India, for the award of the RAMANNA fellowship. We thank A. Derory for his contribution to magnetic measurements.

Supporting Information Available: X-ray crystallographic files in CIF format, bond distance and angle table, bond valence sum table, powder X-ray diffraction patterns, IR, TGA, and figures for the coordination modes of OBA and OBAH. This material is available free of charge via the Internet at http://pubs.acs.org.

JA9017539